Selective Oxidation of Methanol to Dimethoxymethane over Mesoporous Al-P-V-O Catalysts

Shuang Chen, Yali Meng, Yujun Zhao, Xinbin Ma, and Jinlong Gong
Key Laboratory for Green Chemical Technology of Ministry of Education, School of Chemical Engineering and Technology, Tianjin University, Tianjin 300072, P.R. China

DOI 10.1002/aic.14033
Published online March 12, 2013 in Wiley Online Library (wileyonlinelibrary.com)

The synthesis and application of bifunctional mesoporous Al-P-V—O catalysts with both acidic and redox sites for selective oxidation of methanol to dimethoxymethane (DMM) is described. The catalysts were characterized by N_2 adsorption/desorption, X-ray diffraction, temperature-programmed desorption, X-ray photoelectron spectroscopy, and infrared spectroscopy. It is shown that porosity; redox property and surface acidity of the catalysts were greatly influenced by the Al/V/P ratio. The synergistic effect of phosphorus and vanadium was investigated. Al-P-V—O catalysts exhibited good catalytic activity because of the controlled reducibility and the acidic sites. © 2013 American Institute of Chemical Engineers *AIChE J*, 59: 2587–2593, 2013

Keywords: mesoporous Al-P-V—O, methanol oxidation, dimethoxymethane, acidic site, oxygen vacancy

Introduction

Dimethoxymethane (DMM) is an important chemical reagent.[1] It has been widely used as a diesel fuel additive and as an excellent solvent in pharmaceutical and perfume industries due to its low toxicity.[2] DMM is traditionally produced by condensation of formaldehyde and methanol over acidic catalysts; the process comprises complicated procedures, high-reaction temperature, and equipment corrosion. Therefore, one-step selective oxidation of methanol to DMM has attracted much attention considering economic and environmental advantages of the process.

Selective oxidation of methanol to DMM typically involves two steps: oxidation of methanol to formaldehyde on redox sites and condensation of formaldehyde with another methanol molecular to DMM on acidic sites.[3] A variety of catalysts such as supported rhenium oxide,[4] $SbRe_2O_6$,[5] heteropolyacids,[6] Cu-ZSM-5,[7] and V_2O_5/TiO_2 (VT) catalysts[8,9] have been reported active for the reaction. Of particular interest is the development of multicomponents metal oxide catalysts. Royer et al. recently have obtained a methanol conversion of 63% and a DMM selectivity of 89.2% over $Mo_{12}V_3W_{1.2}Cu_{1.2}Sb_{0.5}O_x$ catalyst at 553 K.[10] FeMo catalyst with high-methanol partial pressures also exhibited high yield of DMM (4.6 kg DMM h^{-1} $kgcat^{-1}$, 553 K).[11] High DMM yield is determined by an appropriate balance between reducibility of the oxide and the number of the acidic sites.

Recently, various mesoporous oxo-metallo-phosphates have been synthesized as high-surface-area redox catalysts, possessing tailor-made surface characteristics such as porosity and acidity.[12–14] Indeed, as this type of material is commonly used in acidic, alkaline and redox catalytic process, it could be favorable for the selective oxidation of methanol to DMM. Additive metals such as V, Nb, Mg, Ni, Ti and Al into mesoporous phosphates can influence the structure and surface properties of the material.[15–18]

Oxidation of methanol has also been investigated over V-containing metal oxides catalysts.[19,20] In this work, we have introduced V into oxo-metallo-phosphates to synthesize the mesoporous Al-P-V—O catalysts for the high-redox capacity of vanadium oxide and the acidity of the phosphate material. Acidic and redox properties as well as the structure of the Al-P-V—O catalysts with different Al/V/P ratio were characterized by N_2 adsorption/desorption, X-ray diffraction (XRD), infrared spectra (FTIR), NH_3-TPD, O_2-TPD, and X-ray photoelectron spectroscopy (XPS). The effect of phosphorus and vanadium on the porosity and surface properties was also investigated.

Experimental

Catalysts preparation

Al-P-V—O catalysts were prepared by a coprecipitation method. Calculated amounts of $Al(NO_3)_3 \cdot 9H_2O$ (Kermel, 99%), $(NH_3)_2HPO_4$ (Kermel, 99%) and NH_4VO_3 (Kermel, 99%) dissolved in 200 mL distilled water. An ammonia solution (Kermel, NH_3 25%) was then added gradually under stirring to reach a pH of 9.5. The formed gel was dried at 383 K for 24 h and then calcined in air at 873 K for 6 h. The chemical compositions of the catalysts were analyzed by the ICP-AES. The catalysts were named as AlP_xV_y, where x and y range from 0 to 20 mol %.

Since supported vanadia catalysts have been commonly investigated in this system, for comparison purpose, a reference V-P/Al_2O_3 supported catalyst (5 mol % of P and

Correspondence concerning this article should be addressed to J. L. Gong at jlgong@tju.edu.cn.

20 mol % of V) was also prepared by an impregnation method using ammonia vanadate (NH_4VO_3) and $(NH_3)_2HPO_4$ as metal precursors. The γ-Al_2O_3 support (Jianzhong Co., Ltd., ~135 m^2/g, 200 mesh) was impregnated in the solution under stirring for 5 h. The resultant solids were dried at 383 K for 2 h and then calcined in air at 873 K for 6 h.

Catalytic reactions

Catalytic tests were carried out at the atmospheric pressure in a fixed-bed microreactor made of quartz with an inner diameter of 6 mm. Methanol was introduced into the reaction zone by bubbling O_2/N_2 (1/3 vol, 99.99%) through a glass saturator filled with methanol (99.9%) at 288 K (the MeOH partial pressure is ~9.75 kPa) and kept a gas hourly space velocity (GHSV) of 4,000 h^{-1}. In each test, 0.3 g of catalyst was loaded. The reaction temperature was ranged from 363 K to 673 K. Reaction products were analyzed by an online gas chromatography (SP-2100) using a Propack T column connected to a FID detector and a TCD detector. The FID line allows one to analyze methanol, methyl formate (MF), formaldehyde (FA), dimethyl ether (DME) and dimethoxymethane (DMM), while the TCD line can quantify carbon monoxide (CO) and carbon dioxide (CO_2). The gas lines were kept at 373 K to prevent condensation of the reactant and products.

Catalyst characterization

XRD patterns were collected on a D/Max-2500 diffractometer using C-filtered Cu Kα radiation. It was operated at 40 kV and 200 mA, scanning from 5 to 90° (2θ) at a rate of 0.02°/s.

FTIR spectra were recorded on a Nicolet-6700 FTIR spectrophotometer with a DTGS detector. The spectra were obtained in the 4000–400 cm^{-1} range with a resolution of 4 cm^{-1} and 128 scans. In each experiment, a self-supporting wafer (18 mm dia.) made of 2 mg sample were mixed with 198 mg KBr. The samples were fresh catalysts vacuum-dried at 393 K for 4 h before any measurements.

N_2 adsorption/desorption analysis was performed at 77 K using a Micromeritics Tristar 300 apparatus. The specific surface area was determined by the Bruauer-Emmett-Teller (BET) method. The pore parameters (pore volume and pore diameter) were evaluated from the desorption branch of isotherms based on Barrett-Joyner-Halenda (BJH) model.

NH_3-TPD and O_2-TPD spectra were recorded on a 2910 Chemisorption instrument (Micromeritics). The catalyst (100 mg) was pretreated at 673 K under Ar flow (30 mL min^{-1}) for 1 h, and was then cooled down to 333 K. NH_3 (or O_2) was then introduced into the flow system for 30 min. The TPD spectra were recorded at a ramp rate of 10 K min^{-1} from 333 K to 973 K under He flow.

Temperature-programmed reduction (TPR) measurements were carried out in a continuous mode using a U-type quartz microreactor equipped with a thermal conductivity detector (TCD). The sample (50 mg) was pretreated at 673 K under Ar flow (30 mL min^{-1}) for 1 h, and cooled to room temperature. The sample was then contacted with a H_2: Ar mixture (10 vol % H_2) at a flow rate of 40 mL min^{-1} and heated at a rate of 10 K min^{-1} from room temperature to 1100 K.

XPS measurements were performed on a PHI-1600 instrument (Physical Electronics) equipped with a hemispherical electron analyzer and an Mg Kα X-ray source (1253.6 eV). The samples were fresh catalysts vacuum-dried at 393 K for 4 h before any measurements. The energy region of the photoelectrons was scanned at a passing energy of 29.35 eV. The binding energies were referenced to the C_{1s} band at 284.6 eV. The data was processed using the PHI Multipack Program, Gauss.

Results

Structural properties

We first examine textural properties of catalysts by N_2 adsorption/desorption analysis and the results are listed in Table 1. Al-P-V—O catalysts are mesoporous with an average pore diameter of 4–15 nm. These catalysts displayed high BET surface areas of 200–350 m^2/g, significantly larger than V-P/Al_2O_3. Upon increasing the loading of P, the pore volume and average pore diameter both increased.

XRD spectra were obtained to investigate the changes in crystal structure of the catalysts (Figure 1). The impregnated V-P/Al_2O_3 exhibits a typical crystal structure of γ-Al_2O_3. For Al-P-V—O catalysts, at low content of V and P, only γ-Al_2O_3 characteristic peaks appeared in XRD patterns. For high V contents (e.g., Figure 1g), small peaks around $2\Theta = 20$–30° were detected and ascribed to the formation of V_2O_5.[21] On increasing P contents, an $AlPO_4$ crystal phase (e.g., for $AlP_{20}V_{10}$) becomes detectable with a broad peak at 25°.[22] With the increase of V and P content, the peak intensity of crystalline γ-Al_2O_3 decreased significantly, which indicates the formation of the less crystal but more amorphous phase.

Structure of the catalysts was then characterized by IR spectroscopy to provide information on the various metal-oxygen vibration bands of the catalysts. As shown in Figure 2a, the bands at 772 and 588 cm^{-1} originated from ν(Al-O) vibration are the characteristic peaks of the γ-Al_2O_3 framework.[23] V-P/Al_2O_3 (Figure 2b) remains the framework of γ-Al_2O_3 and the ν(P═O) vibration appeared at the band 1127 cm^{-1}.[24] The peak at 723 cm^{-1} was assigned to ν(V═O) vibration of V_2O_5.[25] However, for Al-P-V—O catalysts (e.g., Figure 2c–f) with similar V/P content of V-P/Al_2O_3, the intensity of γ-Al_2O_3 characteristic peaks decreased obviously, this is corresponded to less crystalline γ-Al_2O_3. The new band at 912 cm^{-1} corresponded to the ν(V—O) vibration of V—O—Al band that with the interaction of V and Al and influenced the original crystal structure.[25] With an increase in P content, the intensity of band 1127 cm^{-1} for ν(P═O) vibration was enhanced. The band at 675 cm^{-1} in Figure 2f–h can be assigned to the ν(Al-O) vibration of the Al-P—O

Table 1. Textural Properties of Catalysts

Sample	BET Surface Area/m^2g^{-1}	BJH Pore Volume/cm^3g^{-1}	BJH Average Pore Diameter/nm
AlP_0V_{20}	271	0.38	4.4
AlP_5V_0	316	0.45	4.3
$AlP_{2.5}V_{10}$	283	0.39	4.4
AlP_5V_{10}	321	0.50	4.6
AlP_5V_{15}	347	0.50	4.6
AlP_5V_{20}	253	0.38	6.0
$AlP_{10}V_{10}$	272	0.73	8.4
$AlP_{10}V_{15}$	272	0.74	8.4
$AlP_{10}V_{20}$	210	0.76	11.5
$AlP_{20}V_{10}$	226	0.91	15.2
V-P/Al_2O_3	114	0.21	5.9

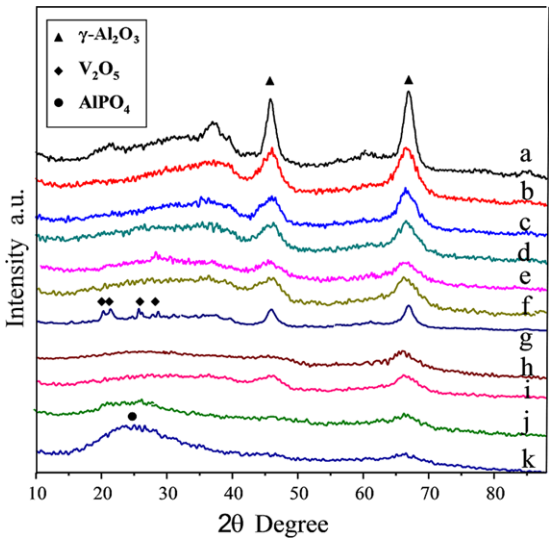

Figure 1. XRD patterns of catalysts.

(a) V-P/Al_2O_3, (b) AlP_0V_{20}, (c) AlP_5V_0, (d) $AlP_{2.5}V_{10}$, (e) AlP_5V_{10}, (f) AlP_5V_{15}, (g)AlP_5V_{20}, (h) $AlP_{10}V_{10}$, (i) $AlP_{10}V_{15}$, (j) $AlP_{10}V_{20}$, and (k) $AlP_{20}V_{10}$. [Color figure can be viewed in the online issue, which is available at wileyonlinelibrary.com.]

species. It is consistent with the results of XRD that incorporation of vanadium and phosphorus may decrease the crystallinity of γ-Al_2O_3 phase and lead to the increased amounts of amorphous structures.

Catalytic reactivity

Performance of catalysts with different composition for methanol oxidation was tested at 383 K and the results are shown in Table 2. The reactivity is apparently dependent on the content and relative ratio of Al/V/P. Catalysts without vanadium (i.e., AlP_5V_0) or phosphorus (i.e., AlP_0V_{20}) exhibited low catalytic activities since both lacks one of the two active sites required for producing DMM (to be discussed later). Upon adding V and P, the methanol conversion increased. However, at high P contents (e.g., $AlP_{20}V_{10}$), the methanol conversion and DMM selectivity decreased. Thus, catalysts with various V and P content exhibited obviously different

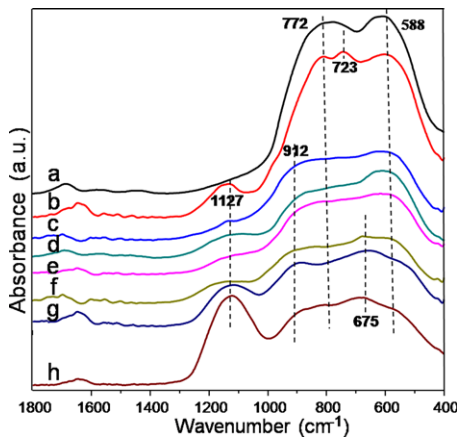

Figure 2. FT- IR spectra of catalysts.

(a) γ-Al_2O_3, (b) V-P/Al_2O_3, (c) AlP_0V_{20}, (d) AlP_5V_0, (e) AlP_5V_{10}, (f) AlP_5V_{15}, (g) $AlP_{10}V_{10}$, and (h) $AlP_{20}V_{10}$. [Color figure can be viewed in the online issue, which is available at wileyonlinelibrary.com.]

Table 2. Catalytic Activities in the Methanol Oxidation Reaction[a]

Sample	Methanol Conversion (%)	Selectivity (%)			
		DMM	DME	MF	FA
AlP_0V_{20}	24.0	71.0	8.5	20.1	0.4
$AlP_{2.5}V_{10}$	35.9	82.3	5.2	12.4	0
AlP_5V_0	12.1	10.0	18.6	71.4	0
AlP_5V_{10}	41.3	64.4	9.0	26.6	0
AlP_5V_{15}	45.5	80.1	6.2	13.6	0.1
AlP_5V_{20}	46.4	87.4	5.6	7.0	1.0
$AlP_{10}V_{10}$	32.1	55.5	10.1	32.4	0
$AlP_{10}V_{15}$	47.3	89.1	5.0	5.9	0
$AlP_{10}V_{20}$	55.6	81.5	6.2	12.3	0
$AlP_{20}V_{10}$	30.6	57.2	7.9	33.9	1.0
V-P/Al_2O_3	26.9	80.1	5.7	14.2	0

[a]The reaction temperature was 383 K; feed gas O_2/N_2 = 1/3 vol; methanol bubbling at 288 K; GHSV = 4000 h^{-1}.

catalytic activities. Catalysts with the appropriate atom ratio (e.g., 5–10 mol. % of P and 15–20 mol. % of V) were favorable for the selective oxidation of methanol to DMM, probably due to the proper structure that balanced acidic and redox sites of the catalysts.[26] The relationship between acidic-redox properties and activity of methanol oxidation will be discussed later.

As the reaction temperature influences the activation of reagents, we have examined reactivity of $AlP_{10}V_{20}$ as a function of temperature and results are listed in Table 3. The $AlP_{10}V_{20}$ catalyst exhibited low-catalytic activity at low temperature (363 K). Upon increasing the temperature to 383 K, methanol conversion increased significantly and the DMM selectivity reached the maximum. With further increasing temperature, the methanol conversion reduced to ~30%, accompanying with a rapid decline in DMM selectivity. As the temperature increased, the amount of the reactants adsorbed on the catalyst surface was gradually reduced, thereby the reaction rate decreased.[10,27] Since the methanol oxidation is an exothermic reaction, the increase in reaction temperature cause a negative effect on selectivity of products. Indeed, a large number of byproducts such as methyl formate and dimethyl ether were formed at high temperatures. It could be due to that high-reaction temperatures facilitate the formation of MF and DME instead of DMM.[28]

Surface acidity

NH_3-TPD was carried out to characterize the surface acidic properties of the catalysts. Figure 3 reveals the strength and distribution of surface acidic sites of the catalysts. As all the catalysts possess strong and weak acidic sites, NH_3-TPD profiles of each catalyst could be deconvolved into these two components. Strong acidic sites can be

Table 3. Catalytic Performance at Different Temperature Over $AlP_{10}V_{20}$[a]

Temperature (K)	Methanol Conversion (%)	Selectivity (%)			
		DMM	DME	MF	FA
363	25.7	65.5	7.7	26.8	0
383	55.6	81.5	6.2	12.3	0
403	44.7	67.2	6.3	24.5	2.0
423	29.4	56.3	6.9	36.8	0
443	31.2	35.3	5.6	59.1	0
473	34.6	14.5	14.4	70.3	0.8

[a]Feed gas O_2/N_2 = 1/3 vol; methanol bubbling at 288 K; GHSV = 4000 h^{-1}.

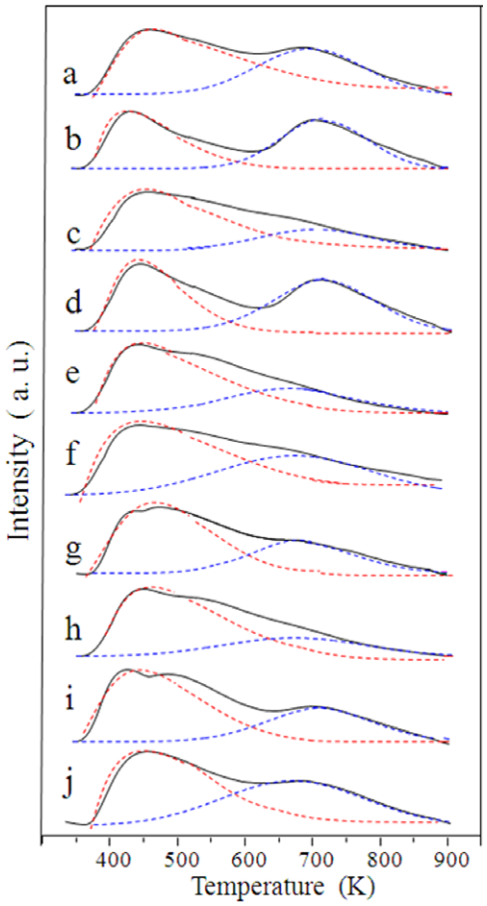

Figure 3. NH_3-TPD profiles of the catalysts with each profile deconvolved by two different components and attributed to weak and strong acidic sites.

(a) AlP_0V_{20}, (b) AlP_5V_0, (c) $AlP_{2.5}V_{10}$, (d) AlP_5V_{10},(e) AlP_5V_{15}, (f) AlP_5V_{20}, (g) $AlP_{10}V_{10}$, (h) $AlP_{10}V_{15}$, (i) $AlP_{10}V_{20}$, and (j) $AlP_{20}V_{10}$. [Color figure can be viewed in the online issue, which is available at wileyonlinelibrary.com.]

quantified via the amount of ammonia desorbed at a high-temperature range (600–900 K), whereas weak acidic sites at a temperature between 300 K and 600 K. It is clear that the acidic sites distribution of the catalysts varies with different ratio of Al/V/P. Particularly, we note that the number of strong acidic sites changes as the content of V and P vary. For curves e-h, which correspond to the catalysts with 5–10 mol. % of P and 15–20 mol. % of V, the change in the amount of the strong acid is less apparent. Comparatively, catalysts with both higher and lower V/P molar ratios possess more strong acid sites.

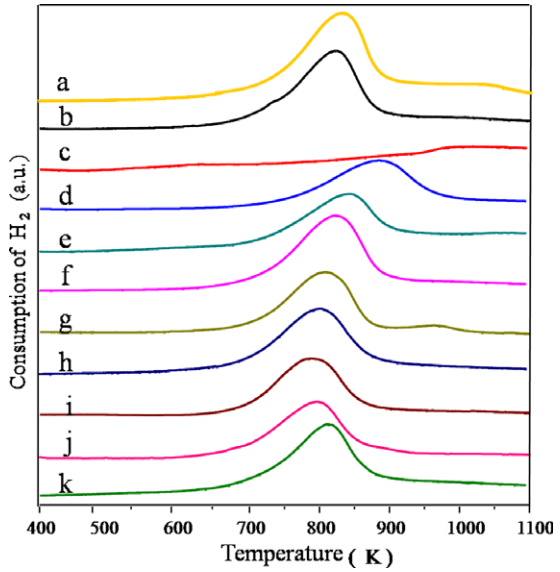

Figure 4. H_2—TPR profiles of catalysts.

(a) V-P/Al_2O_3, (b) AlP_0V_{20}, (c) AlP_5V_0, (d) $AlP_{2.5}V_{10}$, (e) AlP_5V_{10}, (f) AlP_5V_{15}, (g)AlP_5V_{20}, (h) $AlP_{10}V_{10}$, (i) $AlP_{10}V_{15}$, (j) $AlP_{10}V_{20}$, and (k) $AlP_{20}V_{10}$ [Color figure can be viewed in the online issue, which is available at wileyonlinelibrary.com.].

Redox properties

As the first step of methanol oxidation to DMM is to form formaldehyde on redox sites, the redox properties of the catalysts are important to examine. TPR is frequently used to study the redox properties of metal oxides. H_2—TPR profiles of the Al-P-V—O catalysts are shown in Figure 4. AlP_5V_0 catalyst showed weak redox ability, since no H_2 consumption peak was found. Peaks for H_2 consumption around 700–1000 K were observed on other Al-P-V—O catalysts. With the increasing of V loading, the temperature of the maximum of the peak (T_{max}) shifted to a lower value, suggesting the improved reducibility of the catalysts. Increasing the P content also leaded to lower T_{max}. However, for the $AlP_{20}V_{10}$ catalyst with high P content, T_{max} of the main H_2 consumption peak shifted to higher values at ~820 K, indicating that appropriate amount of P can enhance the redox properties of

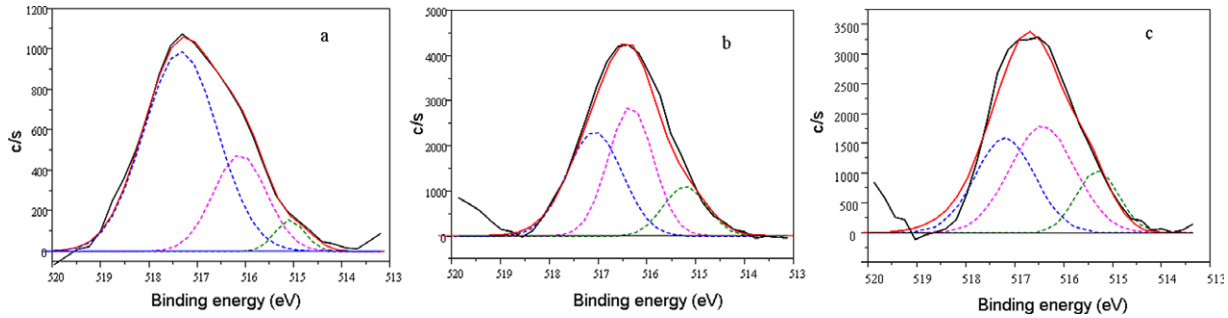

Figure 5. Curve-fitting of the $V_{2p3/2}$ photoelectronic peak of catalysts.

The single components at BE = 517.5, 516.5 and 515.3 eV are plotted as dotted curves and are attributed to V^{5+} phosphate, $V^{5+}$and V^{4+} oxide species, respectively. (a V-P/Al_2O_3, b $AlP_{10}V_{20}$, and c AlP_5V_{20}). [Color figure can be viewed in the online issue, which is available at wileyonlinelibrary.com.]

Table 4. Results of $V_{2p3/2}$ Photoelectron Spectrum Peak-Fitting

Sample	BE (eV)	Oxidate State	Area (%)
V-P/Al_2O_3	515.3	V^{4+}	13.4
	516.5	V^{5+}	36.8
	517.5	V^{5+} in V-P-O	49.8
$AlP_{10}V_{20}$	515.3	V^{4+}	15.5
	516.5	V^{5+}	42.2
	517.5	V^{5+} in V-P-O	42.3
AlP_5V_{20}	515.3	V^{4+}	16.8
	516.5	V^{5+}	43.7
	517.5	V^{5+} in V-P-O	39.5

the catalyst but the excessive amount of P made the catalyst harder to reduce.

The oxidation state and surface content of vanadium species have been analyzed by the $V_{2p3/2}$ peak-fitting from XPS spectra which are shown in Figure 5. The $V_{2p3/2}$ peak of catalysts could be deconvolved by three different components at 515.3 eV, 516.5 eV and 517.5 eV, which are assigned to V^{4+}, V^{5+}, and V^{5+} species in V-P-O, respectively.[29–31] Results of $V_{2p3/2}$ photoelectron spectrum peak-fitting are listed in Table 4. By changing the ratio of Al/V/P, the distribution of vanadium species in different oxidation state also changed.

To understand the active site of the catalytic oxidation, O_2-TPD was taken to characterize the nature of surface oxygen of the catalyst (Figure 6). Two kinds of oxygen desorption peaks appeared at 400–500 K and 550–900 K, respectively. The low-temperature O_2 desorption peak was generally denoted as the weak adsorption of molecular oxygen and O^{2-} on the catalyst surface, while the high-temperature desorption peak represented the oxygen species released from the oxide lattice.[32–34] With the same vanadium content, the oxygen desorption peaks of Al-P-V—O catalysts shifted to the higher temperature compared to the V-P/Al_2O_3 catalyst, and the total amount of oxygen desorption increased as well. This result suggests an enhanced oxygen adsorption capacity of Al-P-V—O catalyst, which would leads to more oxygen species in Al-P-V—O catalyst accessible to the reactants.

As the vanadium oxide is the major redox centers of the catalyst, we compare the catalysts with the same vanadium content (e.g., AlP_5V_{20} and $AlP_{10}V_{20}$) to reflect the influence of phosphorus on redox properties. Compared Figure 6c to 6b, the oxygen desorption temperatures of $AlP_{10}V_{20}$ shifted to higher temperatures with increasing P content and the peak area also increased correspondingly. This indicates that increasing phosphorus content can enhance the oxygen adsorption of the catalyst and increase the amount of lattice oxygen, which would provide more active oxygen sites for the catalytic reaction.

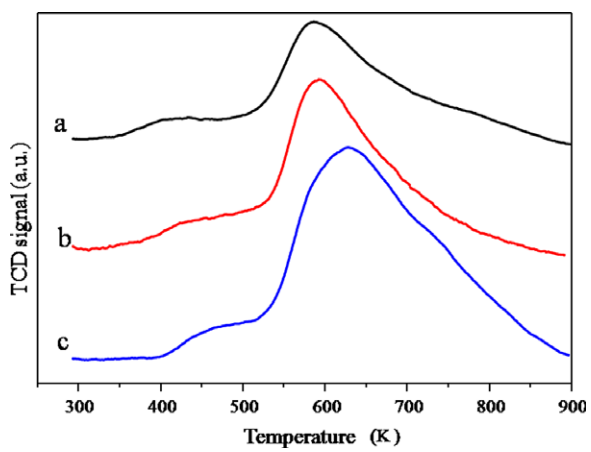

Figure 6. O_2 -TPD profiles of catalysts.

(a) V-P/Al_2O_3, (b) AlP_5V_{20}, and (c) $AlP_{10}V_{20}$. [Color figure can be viewed in the online issue, which is available at wileyonlinelibrary.com.]

Discussion

Structural properties of the catalysts have been characterized by BET, XRD and FTIR. Al-P-V—O catalysts are mesoporous with large surface area. It is clear that upon increasing the P content, the pore volume and the average pore diameter significantly increased. As also reported by Kolonia,[22] the presence of phosphorus species may transform the crystalline alumina into an amorphous state.

It was confirmed by XRD that with the increase of V and P content, the peak intensity of γ-Al_2O_3 decreased gradually, which indicates that introducing of V and P resulted in a formation of less crystalline γ-Al_2O_3 solids and/or the increased amounts of amorphous material. However, this influence of V is relatively weaker compared to phosphorus species. FTIR spectra showed the similar results that the P and V can incorporate with aluminum oxide, leading to formation of the amorphous state.[35]

It is known that methanol is converted to formaldehyde on redox sites, to dimethyl ether (DME) on acidic sites, and to DMM and MF on bifunctional sites.[36] Figure 3 showed that the ratio of Al/V/P influenced both the amount and strength of acidic sites of the catalysts. We have previously shown that a large number of weak acidic sites is required for the DMM production.[19] From NH_3-TPD results and catalytic activity test in this work, the influence on the selectivity of DMM was investigated. In Figure 7, the total yield of MF and DME is related to the number of strong acidic sites obtained from the high-temperature NH_3 TPD peak areas. With the increasing amount of strong acid, the yield of byproduct DME and MF increases. Indeed, strong acidic sites have been reported to favor for the

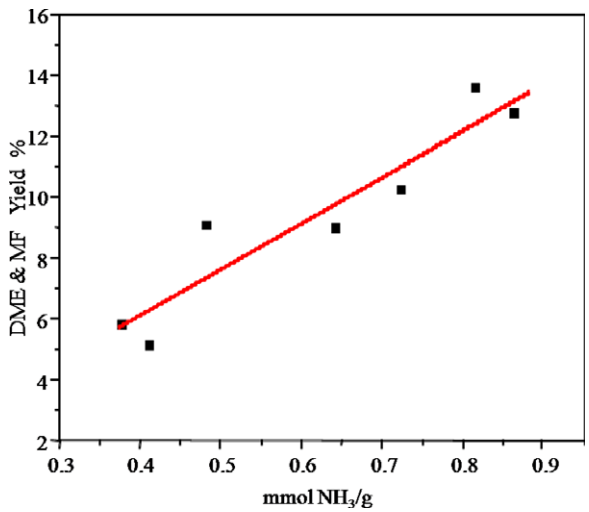

Figure 7. Strong acidic sites correlated with the yield of DME and MF of the catalysts.

[Color figure can be viewed in the online issue, which is available at wileyonlinelibrary.com.]

Table 5. Surface Vanadium Average Oxidation State and Redox Ability

Sample	O_{1s}	$V_{2p3/2}$	V_{ox}	T_{max} (°C)	Methanol Conversion (%)
V-P/Al_2O_3	531.2	517.5	4.5	565	26.9
$AlP_{10}V_{20}$	531.1	516.9	4.1	492	55.6
AlP_5V_{20}	531.1	517.2	4.3	508	46.4

formation of MF and DME[37] which is consistent with this work. Thus, in addition to a large number of acidic sites, strong acidic sites should be restrained to get high DMM selectivity.

As vanadium exhibits different kinds of oxidation states in Al-P-V—O catalyst, the average oxidation state of vanadium (V_{ox}) is used to describe the average valence of the vanadium species in V-P—O materials. This value directly reflects the oxidation state of vanadium on the catalyst surface and is related to the reducibility of the catalysts. V_{ox} can be calculated by the following equation: $V_{ox} = 13.82 - 0.68^{*}(O_{1s} - V_{2p3/2})$.[38] The results of calculated V_{ox} are listed in Table 5.

V_{ox} varies with the ratio of Al/V/P. With the decrease of V_{ox}, the T_{max} of H_2—TPR shifted to lower value, which indicated the enhancement of reducibility. This could lead to the improvement of catalytic activity.

It has been reported that, for methanol oxidation, reactant is typically oxidized to the target product by the lattice oxygen of the catalyst.[39] The reaction follows the Mars-van Krevelen mechanism that is typical of redox chemistry on metal oxides. The continuous supply of oxygen from the bulk to the surface as well as the availability of the oxygen atom in the bridging M-O-support bond would improve the redox capability of the catalyst. Thus, the redox property of the catalyst is greatly influenced by the amount of lattice oxygen and the oxygen mobility of the catalyst.

It was characterized by O_2-TPD that the Al-P-V—O catalysts had large amount of lattice oxygen for the methanol oxidation and high-oxygen adsorption capacity. Gaseous oxygen would be easily adsorbed to the oxygen vacancies, fill the consumed active site, and regenerate the active center to the initial state to complete the redox circle.[40]

Indeed, the mobility of oxygen depends on surface oxygen vacancies.[41,42] According to the XPS results, Al-P-V—O catalysts with lower V_{ox} possessed more oxygen vacancies. Voge et al[43] reported that vanadium and phosphorus oxide can form a substitutional solid solution (close to the vanadyl phosphate complex) which can greatly increase the V^{4+} ratio and was favor to the oxygen adsorption and migration.

The Al-P-V—O catalyst showed good redox properties due to its large amount of lattice oxygen as well as high-absorption capacity and mobility of oxygen, which resulting in the excellent catalytic activity of methanol oxidation.

Conclusions

We have prepared a series of mesoporous Al-P-V—O catalysts by the coprecipitation method that possessed excellent performance in selective oxidation of methanol to DMM. The incorporation of phosphorus and vanadium into γ-Al_2O_3 leaded to the gradual formation of amorphous material with larger surface area. The ratio of Al/V/P determined the existence state of metal oxides, while further influenced the porosity, redox property and surface acidity of the catalysts. Catalytic activity depended on the redox properties of catalyst while the DMM selectivity was greatly influenced by strong acidic sites. The higher DMM yield is obtained because of the better coupled reducibility with the acidic sites, which can be controlled by changing the ratio of Al/V/P of the catalysts. The optimized reaction temperature is 383 K and the proper catalyst composition is 5–10 mol. % of P with 15–20 mol. % of V.

Acknowledgments

The authors are grateful of financial support by the National Science Foundation of China (21006068, 21222604), the Program for New Century Excellent Talents in University (NCET-11-0611), the Scientific Research Foundation for the Returned Overseas Chinese Scholars (MoE), Seed Foundation of Tianjin University (60303002), and the Program of Introducing Talents of Discipline to Universities (B06006).

Literature Cited

1. Masamoto J, Iwaisako T, Chohno M, Kawamura M, Ohtake J, Matsuzaki K. Development of a new advanced process for manufacturing polyacetal resins. Part I. Development of a new process for manufacturing highly concentrated aqueous formaldehyde solution by methylal oxidation. *J Appl Polym Sci*. 1993;50(8):1299–1305.
2. Fuji K, Nakano S, Fujita E. An improved method for methoxymethylation of alcohols under mild acidic conditions. *Synthesis* 1975;4:276–277.
3. Fu Y, Shen J. Selective oxidation of methanol to dimethoxymethane under mild conditions over V_2O_5/TiO_2 with enhanced surface acidity. *Chem Commun*. 2007(21):2172–2174.
4. Yuan YH, Iwasawa Y. Performance and characterization of supported rhenium oxide catalysts for selective oxidation of methanol to methylal. *J Phys Chem B*. 2002;106(17):4441–4449.
5. Yuan YZ, Liu HC, Imoto H, Shido T, Iwasawa Y. Performance and characterization of a new crystalline $SbRe_2O_6$ catalyst for selective oxidation of methanol to methylal. *J Catal*. 2000;195(1):51–61.
6. Liu H, Bayat N, Iglesia E. Site titration with organic bases during catalysis: selectivity modifier and structural probe in methanol oxidation on keggin clusters. *Angew Chem Int Ed*. 2003;42(41):5072–5075.
7. Zhang YH, Drake IJ, Briggs DN, Bell AT. Synthesis of dimethyl carbonate and, dimethoxy methane over Cu-ZSM-5. *J Catal*. 2006;244(2):219–229.
8. Briand LE, Bonetto RD, Sanchez MA, Thomas HJ. Structural modelling of coprecipitated VTiO catalysts. *Catal Today*. 1996;32(1-4):205–213.
9. Bond GC, Tahir SF. Vanadium oxide monolayer catalysts Preparation, characterization and catalytic activity. *Appl Catal*. 1991; 71(1):1–31.
10. Royer S, Secordel X, Brandhorst M, Dumeignil F, Cristol S, Dujardin C, Capron M, Payena E, Dubois JL. Amorphous oxide as a novel efficient catalyst for direct selective oxidation of methanol to dimethoxymethane. *Chem Commun*. 2008(7):865–867.
11. Gornay J, Secordel X, Tesquet G, De Menorval B, Cristol S, Fongarland P, Capron M, Duhamel L, Payen E, Dubois JL, Dumeignil F. Direct conversion of methanol into 1,1-dimethoxymethane: remarkably high productivity over an FeMo catalyst placed under unusual conditions. *Green Chem*. 2010;12(10):1722–1725.
12. Hudson MJ, Knowles JA. Preparation and characterisation of mesoporous, high-surface-area zirconium (IV) oxide. *J Mater Chem*. 1996;6(1):89–95.
13. Ciesla U, Schacht S, Stucky GD, Unger KK, Schüth F. Formation of a porous zirconium oxo phosphate with a high surface area by a surfactant-assisted synthesis. *Angew Chem Int Ed*. 1996;35(5):541–543.
14. Bartley JK, Ellison IJ, Delimitis A, Kiely CJ, Isfahani AZ, Rhodes C, Hutchings GJ. Comparison of vanadium phosphate catalysts derived from $VOPO_4{\cdot}2H_2O$ prepared from H_3PO_4 and $H_4P_2O_7$. *Phys Chem Chem Phys*. 2001;3(20):4606–4613.
15. Holland BT, Isbester PK, Blanford CF, Munson EJ, Stein A. Synthesis of ordered aluminophosphate and galloaluminophosphate mesoporous materials with anion-exchange properties utilizing

polyoxometalate cluster/surfactant salts as precursors. *J Am Chem Soc*. 1997;119(29):6796–6803.
16. Chao ZS, Ruckenstein E. V-Mg-O prepared via a mesoporous pathway: A low-temperature catalyst for the oxidative dehydrogenation of propane to propene. *Catal Lett*. 2004;94(3-4):217–221.
17. Camblor MA, Corma A, Martínez A, Pérez-Pariente J. Synthesis of a titaniumsilicoaluminate isomorphous to zeolite beta and its application as a catalyst for the selective oxidation of large organic molecules. *J Chem Soc Chem Commun*. 1992(8):589–590.
18. Petrakis DE, Pasxalidis I, Theocharis CR, Hudson MJ, Pomonis PJ. Scaling dimensions of nitrogen adsorption characteristics in modulated mesoporous aluminophosphates. *J Colloid Interf Sci*. 1997;185(1):104–110.
19. Chen S, Wang S, Ma X, Gong J. Selective oxidation of methanol to dimethoxymethane over bifunctional VOx/TS-1 catalysts. *Chem Commun*. 2011;47(33):9345–9347.
20. Guo HQ, Li DB, Jiang D, Xiao HC, Li WH, Sun YH. Characterization and performance of V_2O_5-TiO_2 catalysts prepared by rapid combustion method. *Catal Today*. 2010;158(3-4):439–445.
21. Inumaru K, Misono M, Okuhara T. Structure and catalysis of vanadium oxide overlayers on oxide supports. *Appl Catal A: Gen*. 1997;149(1):133–149.
22. Kolonia KM, Petrakis DE, Angelidis TN, Trikalitis PN, Pomonis PJ. Structure and properties of mesoporous alumino-phosphoro-vanadates. *J Mater Chem*. 1997;7(9):1925–1931.
23. Morterra C, Emanuel C, Cerrato G, Magnacca G. Infrared study of some surface properties of boehmite ([gamma]-AlO_2H). *J Chem Soc Faraday Trans*. 1992;88(3):339–348.
24. Andrei ME. IR fundamental spectra and structure of pyrophosphate glasses along the $2ZnO{\cdot}P_2O_5-2Me_2O{\cdot}P_2O_5$ join (Me being Na and Li). *J Non-Cryst Solids*. 1997;209(3):209–226.
25. Magg N, Immaraporn B, Giorgi JB, Schroeder T, Bäumer M, Döbler J, Wu ZL, Kondratenko E, Cherian M, Baerns M, Stair PC, Sauer J, Freund HJ. Vibrational spectra of alumina- and silica-supported vanadia revisited: An experimental and theoretical model catalyst study. *J Catal*. 2004;226(1):88–100.
26. Zhao HY, Bennici S, Shen JY, Auroux A. Nature of surface sites of V_2O_5-TiO_2/SO_4^{2-} catalysts and reactivity in selective oxidation of methanol to dimethoxymethane. *J Catal*. 2010;272(1):176–189.
27. Chen Y, Fierro JLG, Tanaka T, Wachs IE. Supported tantalum oxide catalysts: Synthesis, physical characterization, and methanol oxidation chemical probe reaction. *J Phys Chem B*. 2003;107(22):5243–5250.
28. Liu HC, Iglesia E. Effects of support on bifunctional methanol oxidation pathways catalyzed by polyoxometallate Keggin clusters. *J Catal*. 2004;223(1):161–169.
29. Hatayama F, Ohno T, Maruoka T, Ono T, Miyata H. Structure and acidity of vanadium oxide layered on titania (anatase and rutile). *J Chem Soc Faraday Trans*. 1991;87(16):2629–2633.
30. Bukhtiyarov VI. XPS and SIMS characterization. *Catal Today*. 2000;56(4):403–413.
31. Delichère P, Béré KE, Abon M. Vanadyl pyrophosphate catalysts: Surface analysis by XPS and LEIS. *Appl Catal A Gen*. 1998; 172(2):295–309.
32. Bielanski A, Najbar M. V2O5—MoO3 catalysts for benzene oxidation. *Appl Catal A Gen*. 1997;157(1-2):223–261.
33. Zhaorigetu B, Li W, Xu H, Kieffer R. Correlation between the characteristics and catalytic performance of Ni-V-O catalysts in oxidative dehydrogenation of propane. *Catal Lett*. 2004;94(1):125–129.
34. Liu Y, Jiang C, Chu W, Sun W, Xie Z. Novel F-V_2O_5/SiO_2 catalysts for oxidative dehydrogenation of propane. *React Kinet Mech Catal*. 2010;101(1):141–151.
35. Gougeon RD, Bodart PR, Harris RK, Kolonia DM, Petrakis DE, Pomonis PJ. Solid-state NMR study of mesoporous phosphorovanado-aluminas. *Phys Chem Chem Phys*. 2000;2(22):5286–5292.
36. Badlani M, Wachs IE. Methanol: a "smart" chemical probe molecule. *Catal Lett*. 2001;75(3):137–149.
37. Fu Y, Hong T, Chen J, Auroux A, Shen J. Surface acidity and the dehydration of methanol to dimethyl ether. *Thermochim Acta*. 2005; 434(1):22–26.
38. Coulston GW, Thompson EA, Herron N. Characterization of VPO catalysts by X-ray photoelectron spectroscopy. *J Catal*. 1996;163(1): 122–129.
39. Wang CB, Deo G, Wachs IE. Characterization of vanadia sites in V-silicalite, vanadia-silica cogel, and silica-supported vanadia catalysts: X-ray powder diffraction, Raman spectroscopy, solid-state V-51 NMR, temperature-programmed reduction, and methanol oxidation studies. *J Catal*. 1998;178(2):640–648.
40. Bielański A, Haber J. Oxygen in catalysis on transition metal oxides. *Catal Rev Sci Eng*. 1979;19(1):1–41.
41. Tokarz-Sobieraj R, Witko M, Grybos R. Reduction and re-oxidation of molybdena and vanadia: DFT cluster model studies. *Catal Today*. 2005;99(1-2):241–253.
42. Wachs IE, Weckhuysen BM. Structure and reactivity of surface vanadium oxide species on oxide supports. *Appl Catal A Gen*. 1997;157(1-2):67–90.
43. Voge HH, Adams CR. Catalytic oxidation of olefins. *Advances in Catalysis*. 1967;17:151–221.

Manuscript received Sept. 12, 2012, and revision received Nov. 19, 2012.